



Synthesis of magnetic g-C₃N₄/NiFe₂O₄ nanocomposites for enhanced visible-light photocatalytic performance

Xuemin Chen¹ · Mingli He¹ · Guangyuan He¹ · Yue Zhou² · Jie Ren¹ · Chao Meng²

Received: 4 October 2019 / Accepted: 12 March 2020 / Published online: 25 March 2020
© King Abdulaziz City for Science and Technology 2020

Abstract

A magnetically separable photocatalytic g-C₃N₄/NiFe₂O₄ nanocomposite was obtained via a two-step method. In the first step, the magnetic NiFe₂O₄ nanoparticles were acquired in a few minutes by ionic liquid self-combustion approach which significantly reduced the synthesis time of nanocomposites. Besides, the research of g-C₃N₄/NiFe₂O₄ nanocomposites for the visible-light-driven degradation of methylene blue in the absence of H₂O₂ was detailed. Compared with pure g-C₃N₄ and NiFe₂O₄, the as-prepared nanocomposites with NiFe₂O₄ doping of 12% manifested the enhanced photocatalytic activity and stability after three cycles for degrading methylene blue, and the photocatalytic process followed first-order reaction kinetics. Trapping experiments demonstrated that the H⁺ and OH[•] scavengers are the main active species and O₂^{•-} has a small effect for visible-light-driven degradation of methylene blue.

Keywords g-C₃N₄ · NiFe₂O₄ · Nanocomposite · Photocatalytic properties · Methylene blue · Ionic liquid self-combustion

Introduction

Recently, nano-semiconductor materials have drawn increasing interest in various fields, such as photocatalysis (Fu et al. 2018), photothermal conversion (Chen et al. 2020), heat transfer (Turkyilmazoglu 2019a, b) and electrocatalysis (Gao et al. 2019a, b), and so on. Among them, the research on photocatalysis mainly focuses on the rational design and preparation of semiconductor photocatalysts (Lee et al. 2016; Han et al. 2009). Up to now, various photocatalysts such as TiO₂ (Oseghe and Ofomaja 2018), ZnO (Yu and Yu 2008), BiOX (*x* = Cl, Br, I) (Lei et al. 2019), BiVO₄ (Booshehri et al. 2017), CdS (Mao et al. 2016), g-C₃N₄ (Chidhambaram and Ravichandran 2017) etc. have

been explored for organic degradation, splitting water, and photocatalytic reduction of CO₂. Among these photocatalysts, g-C₃N₄, as a metal-free photocatalyst with a narrow bandgap of ~2.7 eV (Wang et al. 2009), has been widely used for degrading organic pollutants and splitting water for hydrogen production under visible-light irradiation due to its attractive properties, including low cost, simple synthesis method, unique electronic structure, and good stability (Gao et al. 2015; Wang et al. 2012; Ye et al. 2016). Nevertheless, there are still some shortcomings with g-C₃N₄ as photocatalysts because of the low electrical conductivity, deficient utilization of visible light (<460 nm) and rapid recombination rate of charge carriers, which make it poor photocatalytic performance (Chen et al. 2016; Miao et al. 2018; Lam et al. 2016). To overcome these drawbacks, lots of methods have been adopted for improving photocatalytic activity and optical absorption of g-C₃N₄, such as morphology modulation, doping other elements, and combining various semiconductors to construct g-C₃N₄-based heterojunctions or nanocomposites (Liu et al. 2016; Wu et al. 2017; Moreira et al. 2019). Among these strategies, coupling with narrow bandgap semiconductors is a particularly effective approach to restrain the recombination of photo-generated electron–hole pairs and strengthen the visible-light absorption ability, which are crucial to the photocatalytic reaction process (Fang et al. 2019; Wang et al. 2018; Li et al. 2019;

Electronic supplementary material The online version of this article (<https://doi.org/10.1007/s13204-020-01362-6>) contains supplementary material, which is available to authorized users.

✉ Xuemin Chen
chxm0058@163.com

¹ College of Science, Hebei University of Science and Technology, Shijiazhuang 050018, China

² Key Laboratory for Robot and Intelligent Technology of Shandong Province, Shandong University of Science and Technology, No.579 Qianwangang Road, Huangdao District, Qingdao 266590, China

Shi et al. 2018). Moreover, it is still difficult to extend the practical application when using $g\text{-C}_3\text{N}_4$ as photocatalysts due to difficult separation from wastewater and resulting in secondary pollution. Therefore, some efficient efforts have been made to combine $g\text{-C}_3\text{N}_4$ with a magnetic material, such as $g\text{-C}_3\text{N}_4/\text{Fe}_3\text{O}_4$ and $g\text{-C}_3\text{N}_4/\text{MFe}_2\text{O}_4$ ($M = \text{Ni}, \text{Co}, \text{Ca}$ etc.) nanocomposites (Kumar et al. 2013; Hassani et al. 2018; Vadivel et al. 2016), which have showed higher photocatalytic and recycling properties.

In recent years, on account of the photodissolution of iron oxide phase during the photo-degradation process (Beydoun et al. 2000), combining $g\text{-C}_3\text{N}_4$ with spinel MFe_2O_4 has excited interest for photocatalytic field. Unfortunately, there are still some drawbacks: (1) the synthetic strategy of MFe_2O_4 nanomaterials is time consuming (at least 3–5 h) or need high reaction temperature (at least 500 °C) (Liu et al. 2018; Ji et al. 2015; Palanivel et al. 2019), which would affect seriously the synthesis process and yield of $g\text{-C}_3\text{N}_4/\text{MFe}_2\text{O}_4$ nanocomposites; (2) $g\text{-C}_3\text{N}_4/\text{MFe}_2\text{O}_4$ nanocomposites always perform photocatalytic process adding H_2O_2 to organic dye solutions to enhance the photocatalysis activity (Ji et al. 2015; Palanivel et al. 2019; Huang et al. 2015).

Ionic liquid self-combustion synthesis is an attractive technique for the long-scale preparation of different oxides due to its fast process, only a few minutes (Li et al. 2011, 2014, 2015). In the synthesis process, metal nitrates and urea or ammonium nitrate were used as oxidizers and fuels, respectively. Considering the advantage of ionic liquid self-combustion synthesis technique, if the reaction time of MFe_2O_4 nanoparticles is significantly reduced, the long-scale $g\text{-C}_3\text{N}_4/\text{MFe}_2\text{O}_4$ nanocomposites would be gained in a short time. As far as we know, the synthetic process of $g\text{-C}_3\text{N}_4/\text{NiFe}_2\text{O}_4$ (CNNFO) nanocomposites has still consumed long time and CNNFO nanocomposites for the visible-light-driven degradation of methylene blue (MB) in the absence of H_2O_2 has not been studied in previous reports.

In the present work, we acquired CNNFO nanocomposites through a two-step method. Magnetic NiFe_2O_4 nanoparticles in a few minutes by ionic liquid self-combustion synthesis in the first step, which significantly reduced the synthesis time of magnetically separable CNNFO nanocomposites. Then the photocatalytic performance of CNNFO nanocomposites was evaluated through degrading MB in aqueous solution without H_2O_2 under visible-light irradiation and the photocatalytic mechanism was also proposed.

Experimental section

Synthesis of NiFe_2O_4 NPs

To synthesize NiFe_2O_4 NPs, ionic liquid self-combustion synthesis method was used. Typically, 0.01 mol iron(III)

nitrate nanohydrate ($\text{Fe}(\text{NO}_3)_3 \cdot 9\text{H}_2\text{O}$) was mixed with 0.005 mol nickel(II) nitrate hexahydrate ($\text{Ni}(\text{NO}_3)_2 \cdot 6\text{H}_2\text{O}$), 0.003 mol triethylamine hydrochloride ($\text{C}_6\text{H}_{15}\text{NHCl}$), and 0.025 mol urea. Then, the solid mixtures were heated on an electric stove until the formation of homogeneous solutions. After cooling down to room temperature, the NiFe_2O_4 NPs were collected by fully grinding.

Synthesis of $g\text{-C}_3\text{N}_4/\text{NiFe}_2\text{O}_4$ nanocomposites

The CNNFO hybrid nanocomposites with NiFe_2O_4 -doping content of 8–15% were gained by a heating melamine and NiFe_2O_4 method. A typical experiment for the synthesis of 12% CNNFO hybrid nanocomposites was as follows: 5 g of melamine powder and 0.6 g of NiFe_2O_4 were mixed homogeneous by grinding with an agate mortar, and then the mixed powder was put into a porcelain boat and heated to 550 °C for 3 h with a heating rate of 10 °C min^{-1} in air atmosphere. The reddish brown obtained product was collected after grinded with an agate mortar. The pure $g\text{-C}_3\text{N}_4$ product acquired according to the above-mentioned method without NiFe_2O_4 doping.

Characterization

X-ray diffraction (XRD) measurements were carried out on Bruker D8 X-ray diffraction diffractometer with Cu K α radiation. X-ray photoelectron spectroscopy (XPS) analysis was performed using a PHI Quantum 2000 scanning ESCA Microprobe spectrometer. The morphology and structure images were obtained by a Hitachi S-4800 scanning electron microscopy (SEM) and a JEOL-2100 transmission electron microscopy (TEM). The UV–Vis diffuse reflectance spectra (DRS) were recorded on a Hitachi U-4100 spectrometer. The photoluminescence (PL) spectra were observed through a Hitachi F-4600 fluorescence spectrophotometer. It is worth noting that the mass of the $g\text{-C}_3\text{N}_4$ in 12% CNNFO composite should be equal to that of $g\text{-C}_3\text{N}_4$ to fairly compare the PL intensity between $g\text{-C}_3\text{N}_4$ and 12% CNNFO during the PL tests.

Adsorption and photo-degradation experiments

The photocatalytic performance of pure $g\text{-C}_3\text{N}_4$, NiFe_2O_4 , and different mass fraction of CNNFO hybrid nanocomposites was investigated by degrading MB in aqueous solution under visible-light irradiation (300 W Xe lamp with a UV cutoff filter to provide visible light with $\lambda \geq 400$ nm), and the adsorption ability of these samples was assessed through the adsorption experiments of MB in the dark. In a typical procedure, 0.050 g photocatalysts were dispersed into 100 mL of 50 mg L^{-1} MB aqueous solution. First of all, the suspension was stirred in the dark for 0.5 h to ensure

the adsorption/desorption equilibrium of MB on the surface of photocatalysts at room temperature. After that, the lamp was turned on and 4 mL of the suspension was collected in 15 min intervals, centrifuged, and filtered to remove the photocatalysts. Then the concentration of MB was monitored through UV–Vis spectroscopy at 664 nm.

Determination of active species

To probe the active species in the photocatalytic reaction process, 1 mmol L⁻¹ of isopropanol (IPA), 1,4-benzoquinone (BQ), and ammonium oxalate monohydrate (AO) were added into MB solution and utilized as OH[•], O₂^{•-}, and H⁺ scavenger before the photocatalysis process, respectively.

Results and discussion

Structure and morphology properties of photocatalysts

Figure 1 shows the XRD patterns of the as-prepared photocatalysts, including pure g-C₃N₄, NiFe₂O₄, and different mass fraction of CNNFO nanocomposites. For pure g-C₃N₄, the diffraction peaks at 13.1° and 27.4° are assigned to (100) and (002) facets of g-C₃N₄, which represent the in-planar repeat period of the tri-s-triazine units and interlayer-stacking peak of the C–N melon networks, respectively (Ye et al. 2013). For pure NiFe₂O₄, the typical diffraction peaks appear at 18.4°, 30.3°, 35.7°, 37.3°, 43.3°, 53.8°, 57.3°, and 63.0°, which can be matching well with (111), (220), (311), (222), (400), (422), (511), and (440) facets of NiFe₂O₄ (JCPDS 54-0964), respectively (Ji et al. 2015). Notably, the characteristic peaks of Fe₂O₃ or NiO phases were not detected,

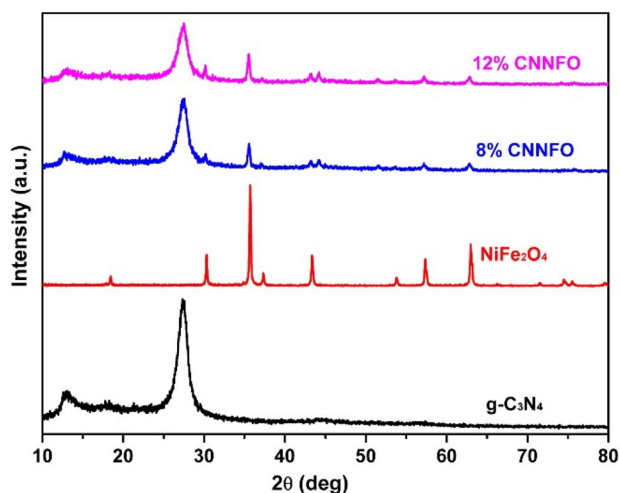


Fig. 1 XRD patterns of pure g-C₃N₄, NiFe₂O₄, 8%, and 12% CNNFO nanocomposites

which illustrates that there is no impurity in the synthesis pathway of NiFe₂O₄. Compared with the pure g-C₃N₄ and NiFe₂O₄, the XRD patterns of 8% and 12% CNNFO nanocomposites appear as the characteristic peaks of both g-C₃N₄ and NiFe₂O₄, which indicates that NiFe₂O₄ nanocrystals have been successfully attached to the g-C₃N₄ nanosheets.

The surface composition and chemical states of the 12 wt% CNNFO nanocomposite were investigated through XPS measurements, and the spectra of as-prepared photocatalysts are shown in Fig. 2. The survey spectra (Fig. 2a) reveal that the hybrid nanocomposite consists of C, N, Ni, Fe, and O elements. The C 1s high-resolution spectra of as-obtained CNNFO nanocomposite (Fig. 2b) shows two obvious peaks at 284.8 and 288.2 eV, which should be assigned to the *sp*² C–C bonds from carbon-containing contaminations and *sp*²-bonded carbon of N–C=N in the graphitic structure, respectively (Liu et al. 2017). Three peaks were resolved in the N 1s resolution spectrum of the nanocomposites (Fig. 2c), which were 398.9, 400.4, and 401.7 eV corresponding to *sp*² hybridized aromatic N atoms (C=N–C), *sp*³ hybridized N atoms (H–N–(C)₃) and C–N–H structure, respectively. In Fig. 3d, the Ni 2*p* spectra of the nanocomposite can be fit into two typical strong peaks at 855.5 and 872.7 eV, which are assigned to 2*p* 3/2 and 2*p* 1/2 of Ni 2*p*, respectively; and two small peaks at 861.7 and 879.6 eV correspond to the satellite peaks of Ni 2*p* 3/2 and Ni 2*p* 1/2, respectively (Zhao et al. 2018). This confirms that the Ni in CNNFO nanocomposite exists in +2 oxidation state. Two strong peaks of Fe 2*p* spectrum at 710.8 and 724.5 eV can be attributed to Fe 2*p* 3/2 and Fe 2*p* 1/2, respectively, which illustrates that the oxidation of Fe in CNNFO nanocomposite is +3 (Zhao et al. 2018). Through deconvolution of the high-resolution O 1s spectra, three peaks at 529.7, 531.0, and 532.2 eV are attributed to the metal–oxygen bonds and oxygen atoms in the hydroxyl groups and absorbed water (Gao et al. 2019a, b).

Figure 3a–c show SEM images of pure g-C₃N₄, NiFe₂O₄, and 12% CNNFO nanocomposites, respectively. The as-prepared g-C₃N₄ (Fig. 3a) is composed of an irregular nanosheet structure, whereas the pure NiFe₂O₄ product consist of nanoparticles with the range of size about 90–200 nm (Fig. 3b). As can be seen from the Fig. 3b, the as-obtained pure NiFe₂O₄ nanoparticles have partly a little agglomeration. Figure 3c displays that NiFe₂O₄ nanoparticles were successfully deposited on g-C₃N₄ nanosheets in the 12% CNNFO nanocomposites, which is consistent with the TEM image of Fig. 3d. The HRTEM image (Fig. 3d-1) confirms that the nanoparticle attaching to the g-C₃N₄ nanosheet in TEM image is identified as NiFe₂O₄ with the (311) crystal face, and the result is also consistent with the SAED image (Fig. 3d-2).

Figure 4a displays the UV–Vis DRS of as-prepared samples, which can illustrate the light absorption ability of the

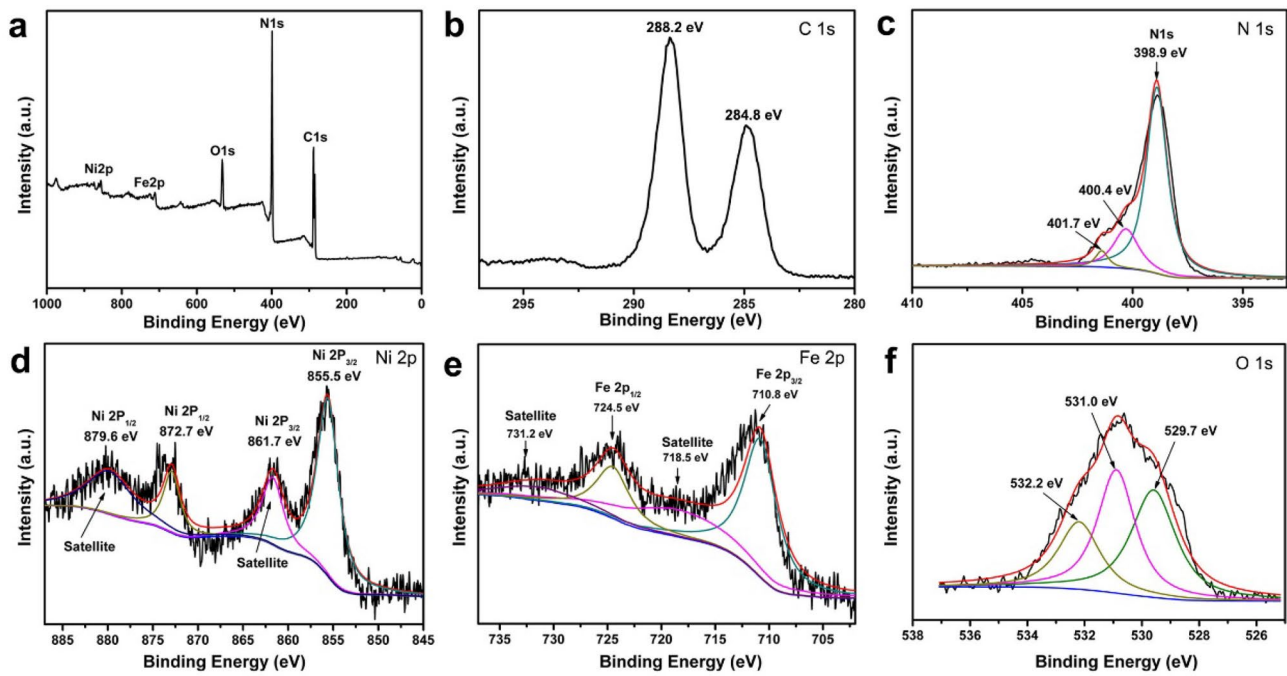
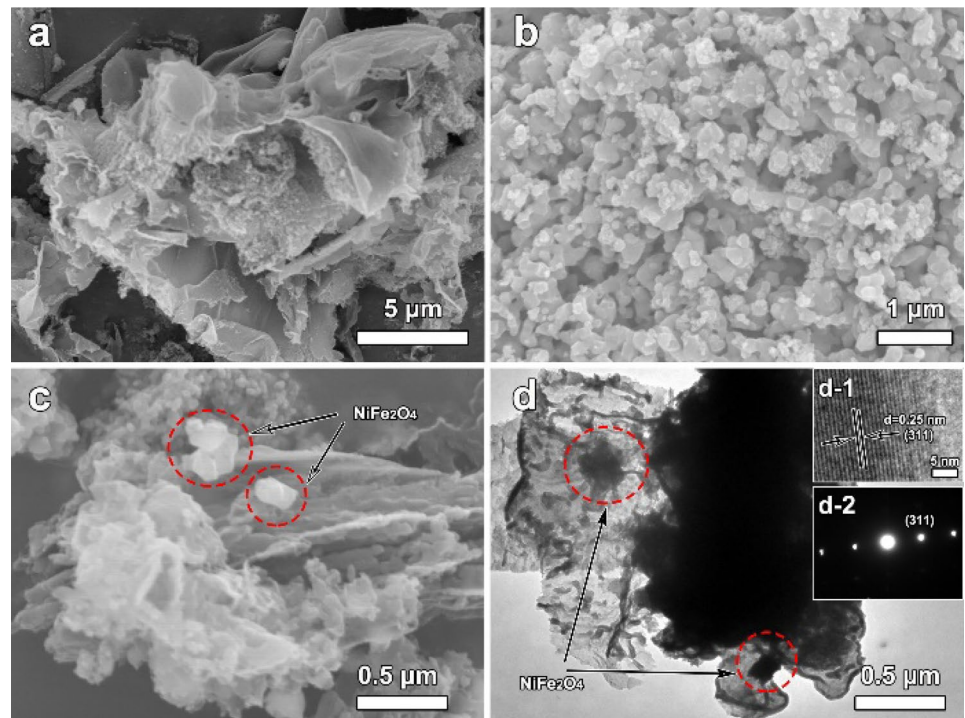


Fig. 2 XPS spectra of 12 wt% CNNFO nanocomposite: **a** survey spectra, **b** C 1s spectra, **c** N 1s spectra, **d** Ni 2p spectra, **e** Fe 2p spectra, **f** O 1s spectra

Fig. 3 SEM images of pure $g\text{-C}_3\text{N}_4$ (**a**), pure NiFe_2O_4 (**b**), and 12% CNNFO composites (**c**). **d** TEM image of 12% CNNFO composites. **d-1** HRTEM image of the NiFe_2O_4 nanoparticles. **d-2** SAED pattern of the NiFe_2O_4 nanoparticles



photocatalysts. It can be seen that the adsorption edge of pure $g\text{-C}_3\text{N}_4$ nanosheets was around 460 nm. However, the CNNFO nanocomposites showed a much stronger absorption in the visible-light range, and a red shift in comparison

with the pure $g\text{-C}_3\text{N}_4$ nanosheets appeared. The enhanced light absorption of the CNNFO nanocomposites may promote the generation of more electron–hole pairs, which will improve the photocatalytic performance. Figure 4b shows

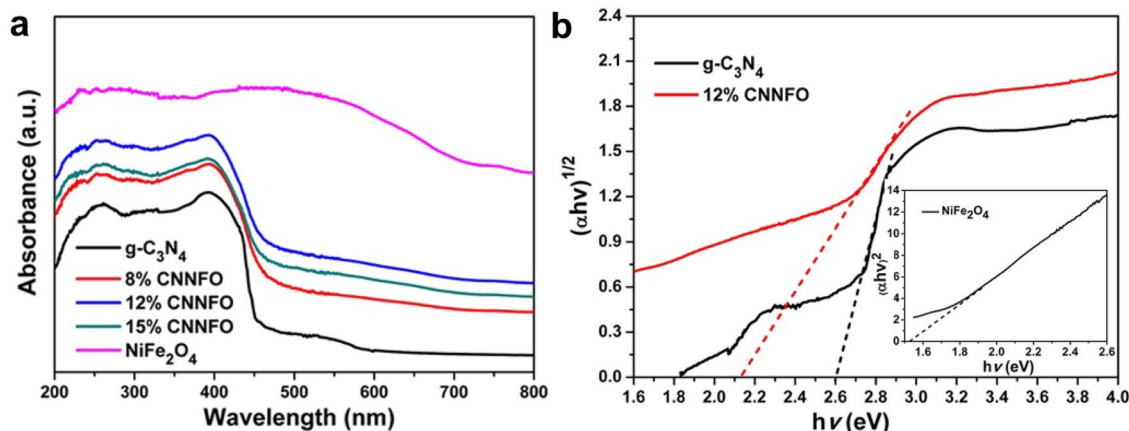


Fig. 4 **a** UV–Vis diffuse reflectance spectra (DRS); **b** bandgap energy of the as-prepared photocatalysts

that the bandgap energy of pure $g\text{-C}_3\text{N}_4$ and NiFe_2O_4 was about 2.6 and 1.53 eV respectively, which corresponded to the above results. When NiFe_2O_4 nanoparticles were introduced to $g\text{-C}_3\text{N}_4$, the energy level of CNNFO would be changed and hence the optical adsorption property could be broadened in visible region. The bandgap of 12% CNNFO nanocomposites ($E_g = 2.14$ eV) is lower than pure $g\text{-C}_3\text{N}_4$.

Photocatalytic performance

The adsorption and photo-degradation performances of the as-prepared samples under visible-light irradiation were evaluated (Fig. 5a). The initial and actual concentration of the MB solution is labeled C_0 and C , respectively. It can be found that the as-prepared samples show excellent adsorptive capacities. Obviously, the adsorption efficiency of the 12% CNNFO nanocomposites reaches to 31.1%, which is the highest adsorption capacity compared to the other samples.

The photo-degradation reaction got under way after the light was switched on to irradiate the photo-degradation system. As shown in Fig. 5a, the decrease of the MB concentration is faster and more effective with the 12% CNNFO nanocomposites than with pure $g\text{-C}_3\text{N}_4$, NiFe_2O_4 , and other ratio of CNNFO nanocomposites. Specifically, the photo-degradation efficiency of MB dye reaches as high as 90% after 45 min irradiation with the 12% CNNFO nanocomposites, and after exposed to visible light for 75 min, the photo-degradation of MB achieves terminus, which can be clearly shown from the image of the MB color change (Fig. 5a inset). Figure 5b displays the plots of $\ln(C/C_0)$ versus irradiation time, which illustrates that the photo-degradation process was a first-order kinetic reaction. As shown in Table 1, the photo-degradation rate of 12% CNNFO was nearly seven times higher than that of pure $g\text{-C}_3\text{N}_4$. Compared with the photo-degradation activity of 12% mechanically mixed sample, the as-prepared 12% CNNFO nanocomposite still shows

the best photo-degradation performance, which directly demonstrated the successful combination of $g\text{-C}_3\text{N}_4$ and NiFe_2O_4 . The UV–Vis DRS results of mechanically mixed sample and 12% CNNFO nanocomposite were shown in Fig. S1. It can also verify the existing interaction between $g\text{-C}_3\text{N}_4$ and NiFe_2O_4 in 12% CNNFO composite, which is in favor of the photocatalytic activity. Due to the magnetism of the 12% CNNFO nanocomposite (Fig. 5c inset), the photocatalyst can be easily separated from the MB dye solution and recycled for the photo-degradation system. Figure 5d shows the 12% CNNFO nanocomposite can keep high photocatalytic capacity after three uses, which illustrates the structure of the photocatalyst was stable.

The mechanism discussion of the enhanced photocatalytic activity

To reveal the mechanism of the photocatalytic performance, the intensity of PL emission spectra of the as-prepared photocatalysts was recorded to characterize the separation efficiency of photo-generated carriers in pure $g\text{-C}_3\text{N}_4$ and mass 12% CNNFO composite. As shown in Fig. 6, the PL peak intensity of 12% CNNFO composite is decreased remarkably compared with that of pure $g\text{-C}_3\text{N}_4$, indicating that the hybridization nanocomposite with NiFe_2O_4 nanoparticles can inhibit the recombination of photo-generated electro-hole pairs compared with the pure $g\text{-C}_3\text{N}_4$. That is, the lifetime of charge carriers in 12% CNNFO is longer than that of pure $g\text{-C}_3\text{N}_4$, which is beneficial for the improvement of photocatalytic activity.

To research the charge transfer and recombination rate of the 12% CNNFO nanocomposites, EIS study was carried out in electrolyte (Fig. 7). As is well known, a smaller radius in a Nyquist plot illustrates a small charge transfer resistance in photocatalytic process. Figure 7 shows that the charge transfer resistance of 12% CNNFO is smaller than

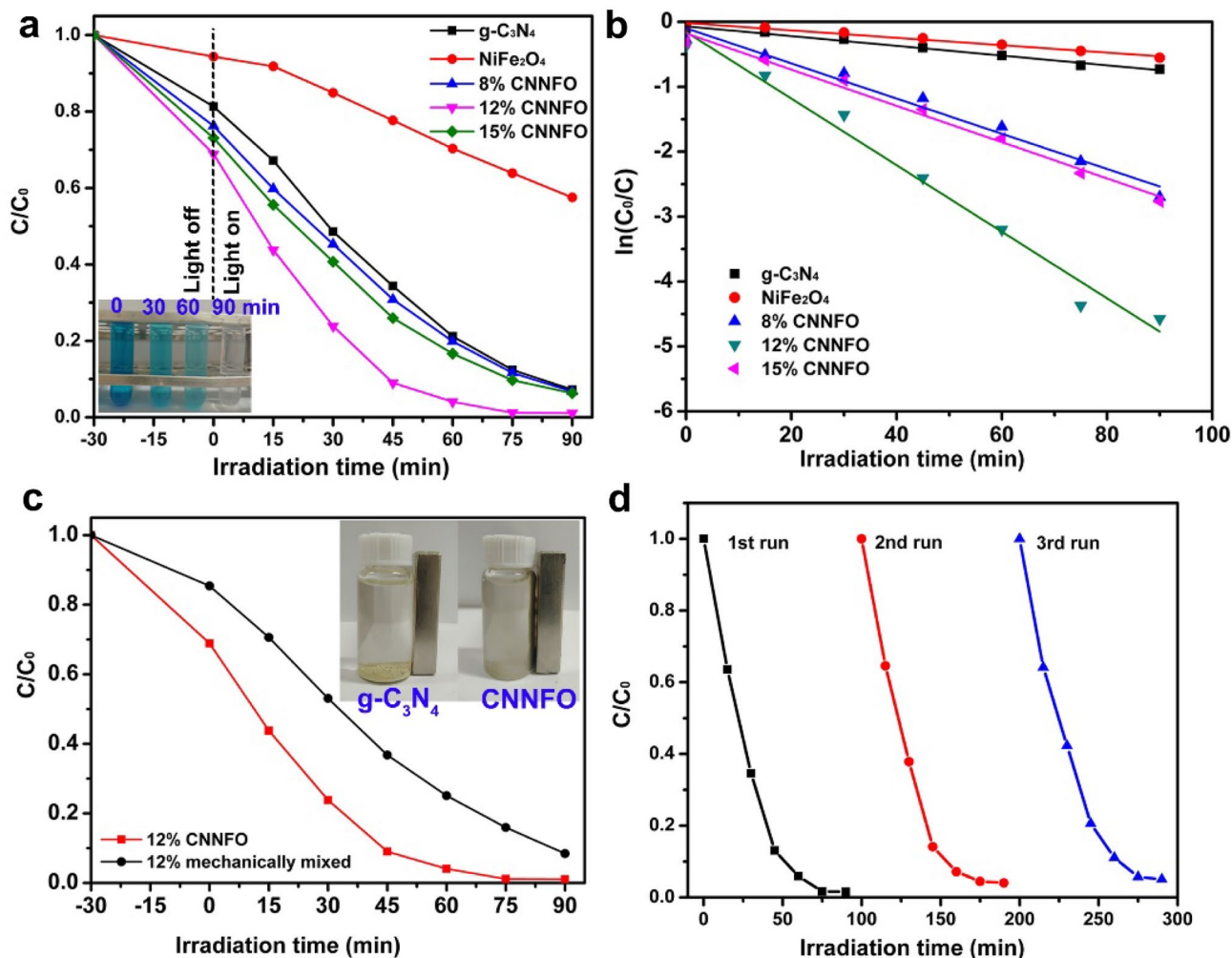


Fig. 5 a Photocatalytic degradation of MB by the as-prepared photocatalysts under visible-light irradiation, the inset shows the MB color change at different irradiation time. b Kinetic fit diagram. c Photocatalytic degradation performance comparison between 12% CNNFO

and 12% mechanically mixed, the inset images show the separation ability of the CNNFO photocatalyst dispersed in water using a permanent magnet. d Recyclability of the 12% CNNFO photocatalyst for the degradation of MB

Table 1 First-order kinetic constant of the photo-degradation process

Samples	k (min ⁻¹)	R^2
g-C ₃ N ₄	0.0075	0.9889
NiFe ₂ O ₄	0.0057	0.9792
8% CNNFO	0.0271	0.9740
12% CNNFO	0.0513	0.9714
15% CNNFO	0.0279	0.9874

the pure g-C₃N₄ under visible-light irradiation, manifesting that a more facile charge transfer occurred in 12% CNNFO nanocomposite. That is, an effective separation and transfer of photo-generated electron–hole pairs appeared in the process of the photo-degradation when 12% CNNFO composites were used as photocatalysts, resulting in enhancing

higher photocatalytic activity. This evidence agrees with the above PL result.

As is well known, the mechanism of photo-degradation pathway can use different scavengers to trap the reactive species such as electrons, holes, OH[•], and O₂^{•-}, which generate in the process of the photo-degradation (Samadi et al. 2019; Padervand 2016). Thus, the photo-catalytic mechanism over 12% CNNFO nanocomposites was explored through the trapping experiments of free radicals and holes. Isopropanol (IPA), 1,4-benzoquinone (BQ) and ammonium oxalate monohydrate (AO) were used as three different scavengers for trapping OH[•], O₂^{•-}, and H⁺ (Hu et al. 2019). Figure 8 shows that the photocatalytic activity had a relatively a little change upon the addition of BQ as a O₂^{•-} scavenger, confirming that O₂^{•-} plays small effect during the photo-degradation process. However, when AO and IPA were

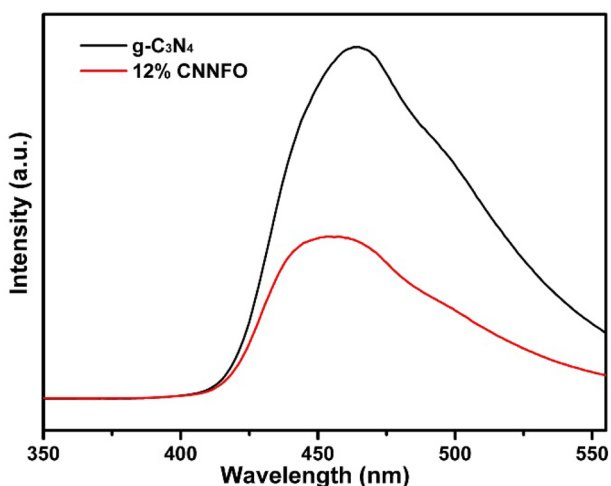


Fig. 6 Room temperature PL spectra of the as-prepared photocatalysts

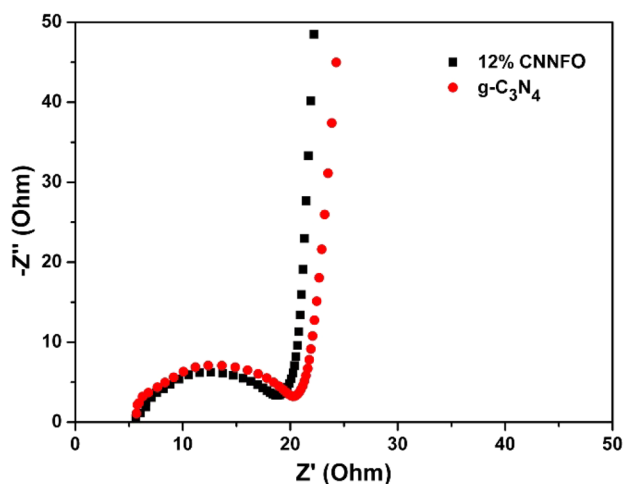


Fig. 7 EIS measurements of pure g-C₃N₄ and 12% CNNFO composite

conducted as hole and OH[•] scavengers, a remarkable change was observed compared with the absence of scavenger under similar conditions, indicating that the H⁺ and OH[•] scavengers are the main active species in the reaction system.

Figure 9 shows the schematic drawing of the MB photodegradation over CNNFO nanocomposites. Under the visible-light irradiation, electrons on the VB position for both g-C₃N₄ and NiFe₂O₄ were excited to the CB position. Due to the lower CB level of NiFe₂O₄, electrons on the CB position of g-C₃N₄ can easily be transferred to the CB of NiFe₂O₄ and holes on the VB position of NiFe₂O₄ were transferred to the VB of g-C₃N₄, which can suppresses the recombination of the photo-induced carriers, leaving more charge carriers as reactive species. The roles of electrons and holes are as follows: the electrons on the NiFe₂O₄ CB react with

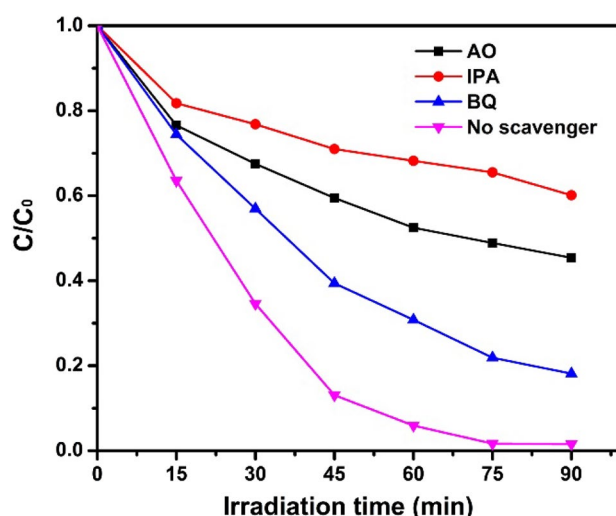


Fig. 8 Active species trapping experiments using a series of scavengers

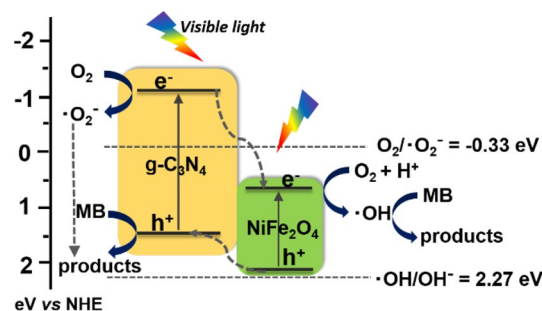


Fig. 9 The proposed mechanism of the reaction process

O₂ and H⁺ to generate OH[•], which serves as a scavenger to degrade MB; because the CB value of g-C₃N₄ is lower than that of O₂/O₂^{•-} (Zhang et al. 2009), the photoactivated electrons on the CB can easily reduce O₂ to O₂^{•-}; the holes directly degrade MB adsorbed on the CNNFO surface. All of reactive species including OH[•], holes, and O₂^{•-} are thus beneficial for the degradation of MB under visible-light irradiation.

Conclusion

In summary, the CNNO nanocomposites were prepared via a two-step method. It is worth noting that the magnetic NiFe₂O₄ nanoparticles were acquired in a few minutes by ionic liquid self-combustion synthesis approach in the first step which significantly reduced the synthesis time of magnetically separable CNNFO nanocomposites, and in the absence of H₂O₂ solution, the CNNFO nanocomposite could still be performed on the enhanced photo-degradation

activity under visible-light irradiation. The reason for this result can attribute to the efficient light absorption and separation of charge carriers. It is believed that the present synthetic route for the magnetically photocatalyst preparation can provide the valuable experimental basis for practical application.

Acknowledgements The authors gratefully acknowledge the financial support of the Natural Science Foundation of Hebei Province, China (Grant no. B2018208090), Young Talents Program in University of Hebei Province, China (no. BJ2019002), the National Natural Science Foundation of China (Grant no. 51802075, 51901115), and the Shandong Provincial Natural Science Foundation, China (ZR2019PEM001 and ZR2019BB009).

Author contributions The manuscript was finished through contributions of all authors. All authors have given approval to the final version of the manuscript.

Compliance with ethical standards

Conflict of interest The authors declare no conflict of interest.

References

- Beydoun B, Amal R, Low GKC, McEvoy S (2000) Novel photocatalyst: titania-coated magnetite. Activity and photodissolution. *J Phys Chem B* 104:4387–4396
- Booshehri AY, Polo-Lopez MI, Castro-Alferez M, He PF, Xu R, Rong W, Malato S, Fernández-Ibáñez P (2017) Assessment of solar photocatalysis using Ag/BiVO₄ at pilot solar compound parabolic collector for inactivation of pathogens in well water and secondary effluents. *Catal Today* 281:124–134
- Chen Y, Lin B, Wang H, Zhu HB, Wl Yu, Basset J (2016) Surface modification of g-C₃N₄ by hydrazine: simple way for noble-metal free hydrogen evolution catalysts. *Chem Eng J* 286:339–346
- Chen XD, Chao M, Yong W, Zhao QQ, Li YJ, Chen XM, Yang DW, Li YX, Zhou Y (2020) Laser-synthesized rutile TiO₂ with abundant oxygen vacancies for enhanced solar water evaporation. *ACS Sustain Chem Eng* 8:1095–1101
- Chidhambaram N, Ravichandran K (2017) Single step transformation of urea into metal-free g-C₃N₄ nanoflakes for visible light photocatalytic applications. *Mater Lett* 207:44–48
- Fang JJ, Chen YK, Wang W, Fang L, Lu CH, Zhu C, Kou JH, Ni YR, Xu ZZ (2019) Highly efficient photocatalytic hydrogen generation of g-C₃N₄-CdS sheets based on plasmon-enhanced triplet-triplet annihilation upconversion. *Appl Catal B Environ* 258:117762
- Fu JW, Yu JG, Jiang CJ, Cheng B (2018) g-C₃N₄-based heterostructured photocatalysts. *Adv Energy Mater* 8:1701503
- Gao SW, Low JX, Yu JG, Jaroniec M (2015) Polymeric photocatalysts based on graphitic carbon nitride. *Adv Mater* 27:2150–2176
- Gao ZW, Liu JY, Chen XM, Zheng XL, Jing M, Liu H, Ma T, Li L, Wang WC, Du XW (2019a) Engineering NiO/NiFe LDH intersection to bypass scaling relationship for oxygen evolution reaction via dynamic tridimensional adsorption of intermediates. *Adv Mater* 31:1804769
- Gao XC, Wang WL, Bi JQ, Chen YF, Hao XX, Sun XN, Zhang JD (2019b) Morphology-controllable preparation of NiFe₂O₄ as high performance electrode material for supercapacitor. *Electrochim Acta* 296:181–189
- Han F, Kambala VSR, Srinivasan M, Rajarathnam D, Naidu R (2009) Tailored titanium dioxide photocatalysts for the degradation of organic dyes in wastewater treatment: a review. *Appl Catal A Gen* 359:25–40
- Hassani A, Eghbali P, Ekicibil A, Metin Ö (2018) Monodisperse cobalt ferrite nanoparticles assembled on mesoporous graphitic carbon nitride (CoFe₂O₄/mpg-C₃N₄): a magnetically recoverable nanocomposite for the photocatalytic degradation of organic dyes. *J Magn Mater* 456:400–412
- Hu JS, Zhang PF, An WJ, Liu L, Liang YH, Cui WQ (2019) In-situ Fe-doped g-C₃N₄ heterogeneous catalyst via photocatalysis-Fenton reaction with enriched photocatalytic performance for removal of complex wastewater. *Appl Catal B Environ* 245:130–143
- Huang SQ, Xu YG, Xie M, Xu H, He MQ, Xia JX, Huang LY, Li HM (2015) Synthesis of magnetic CoFe₂O₄/g-C₃N₄ composite and its enhancement of photocatalytic ability under visible-light. *Colloid Surf A Physicochem Eng Aspects* 478:71–80
- Ji HY, Jing XC, Xu YG, Yan J, Li HP, Li YP, HuangZhangXu LYQH, Li HM (2015) Magnetic g-C₃N₄/NiFe₂O₄ hybrids with enhanced photocatalytic activity. *RSC Adv* 5:57960–57967
- Kumar ST, Kumar B, Baruah A, Shanker V (2013) Synthesis of magnetically separable and recyclable g-C₃N₄-Fe₃O₄ hybrid nanocomposites with enhanced photocatalytic performance under visible-light irradiation. *J Phys Chem C* 117:26135–26143
- Lam SM, Sin JC, Mohamed AR (2016) A review on photocatalytic application of g-C₃N₄/semiconductor (CNS) nanocomposites towards the erasure of dyeing wastewater. *Mater Sci Semicond Process* 47:62–84
- Lee KM, Lai CW, Ngai KS, Juan JC (2016) Recent developments of zinc oxide based photocatalyst in water treatment technology: a review. *Water Res* 88:428–448
- Lei H, Zhang HH, Zou Y, Ding XP, Jia YM, Wang FF (2019) Synergistic photocatalysis/piezocatalysis of bismuth oxybromide for degradation of organic pollutants. *J Alloy Compd* 809:151840
- Li F, Liu Y, Sun ZM, Liu Rh, Kou CG, Zhao Y, Zhao DS (2011) Facile preparation of porous LaFeO₃ nanomaterial by self-combustion of ionic liquids. *Mater Lett* 65:406–408
- Li FT, Wang Q, Wang XJ, Li B, Hao YJ, Liu RH, Zhao DS (2014) In-situ one-step synthesis of novel BiOCl/Bi₂O₃/Cl₁₀ heterojunctions via self-combustion of ionic liquid with enhanced visible-light photocatalytic activities. *Appl Catal B Environ* 150:574–584
- Li FT, Ran JR, Jaroniec M, Qiao SZ (2015) Solution combustion synthesis of metal oxide nanomaterials for energy storage and conversion. *Nanoscale* 7:17590–17610
- Li X, Shen D, Liu C, Li JZ, Zhou YJ, Song XH, Huo PW, Wang HQ, Yan YS (2019) Fabricated rGO-modified Ag₂S nanoparticles/g-C₃N₄ nanosheets photocatalyst for enhancing photocatalytic activity. *J Colloid Interface Sci* 554:468–478
- Liu L, Qi YH, Lu JR, Lin SL, An WJ, Liang YH, Cui WQ (2016) A stable Ag₃PO₄@g-C₃N₄ hybrid core@shell composite with enhanced visible light photocatalytic degradation. *Appl Catal B Environ* 183:133–141
- Liu X, Jin AL, Jia YS, Ti X, Deng CX, Zhu MH, Chen CF, Chen XS (2017) Synergy of adsorption and visible-light photocatalytic degradation of methylene blue by a bifunctional Z-scheme heterojunction of WO₃/g-C₃N₄. *Appl Surf Sci* 405:359–371
- Liu Y, Song YC, You YH, Fu XJ, Wen J, Zheng XG (2018) NiFe₂O₄/g-C₃N₄ heterojunction composite with enhanced visible-light photocatalytic activity. *J Saudi Chem Soc* 22:439–448
- Mao J, Chen XM, Du XW (2016) Facile synthesis of three dimensional CdS nanoflowers with high photocatalytic performance. *J Alloy Compd* 656:972–977
- Miao XL, Yue XY, Ji ZY, Shen XP, Zhou H, Liu MM, Xu KQ, Zhu J, Zhu GX, Kong L, Shah SA (2018) Nitrogen-doped carbon dots decorated on g-C₃N₄/Ag₃PO₄ photocatalyst with improved visible

- light photocatalytic activity and mechanism insight. *Appl Catal B Environ* 227:459–469
- Moreira NFF, Sampaio MJ, Ribeiro R, Silva CG, Faria JL, Silva AMT (2019) Metal-free g-C₃N₄ photocatalysis of organic micropollutants in urban wastewater under visible light. *Appl Catal B Environ* 248:184–192
- Oseghe EO, Ofomaja AE (2018) Facile microwave synthesis of pine cone derived C-doped TiO₂ for the photodegradation of tetracycline hydrochloride under visible-LED light. *J Environ Manag* 223:860–867
- Padervand M (2016) Visible-light photoactive Ag-AgBr/ α -Ag₃VO₄ nanostructures prepared in a water-soluble ionic liquid for degradation of wastewater. *Appl Nanosci* 6:1119–1126
- Palanivel B, Ayappan C, Jayaraman V, Chidambaram S, Maheswaran R, Mani A (2019) Inverse spinel NiFe₂O₄ deposited g-C₃N₄ nanosheet for enhanced visible light photocatalytic activity. *Mater Sci Semicond Process* 100:87–97
- Samadi M, Zirak M, Naseri A, Kheirabadi M, Ebrahimi M, Moshfegh AZ (2019) Design and tailoring of one-dimensional ZnO nanostructures for photocatalytic degradation of organic dyes: a review. *Res Chem Intermediat* 45:2197–2254
- Shi L, Zhao KM, Liu SQ (2018) Photocatalytic degradation of MO and phenol over novel β -CoOOH/g-C₃N₄ composite under visible light irradiation. *Mater Lett* 228:121–124
- Turkyilmazoglu M (2019a) Free and circular jets cooled by single phase nanofluids. *Eur J Mech B Fluid* 76:1–6
- Turkyilmazoglu M (2019b) Fully developed slip flow in a concentric annuli via single and dual phase nanofluids models. *Comput Methods Progr Biomed* 179:104997
- Vadivel S, Maruthamani D, Habibi-Yangjeh A, Paul B, Dhar SS, Selvam K (2016) Facile synthesis of novel CaFe₂O₄/g-C₃N₄ nanocomposites for degradation of methylene blue under visible-light irradiation. *J Colloid Interface Sci* 480:126–136
- Wang XC, Maeda K, Thomas A, Takanabe K, Xin G, Carlsson JM, Domen K, Antonietti M (2009) A metal-free polymeric photocatalyst for hydrogen production from water under visible light. *Nat Mater* 8:76–80
- Wang XC, Blechert S, Antonietti M (2012) Polymeric graphitic carbon nitride for heterogeneous photocatalysis. *ACS Catal* 2:1596–1606
- Wang HH, Peng DL, Hu XF, Ma XG, Ye WH, Zhang WH, Chang Y, Dong SJ (2018) Target preparation of multicomponent composites Au@CdS/g-C₃N₄ as efficient visible light photocatalysts with the assistance of biomolecules. *Mater Res Bull* 108:176–186
- Wu FJ, Li X, Liu W, Zhang ST (2017) Highly enhanced photocatalytic degradation of methylene blue over the indirect all-solid-state Z-scheme g-C₃N₄-RGO-TiO₂ nanoheterojunctions. *Appl Surf Sci* 405:60–70
- Ye S, Qiu LG, Yuan YP, Zhu YJ, Xia J, Zhu JF (2013) Facile fabrication of magnetically separable graphitic carbon nitride photocatalysts with enhanced photocatalytic activity under visible light. *J Mater Chem A* 1:3008
- Ye LQ, Wu D, Chu KH, Wang B, Xie HQ, Yip HY, Wong PK (2016) Phosphorylation of g-C₃N₄ for enhanced photocatalytic CO₂ reduction. *Chem Eng J* 304:376–383
- Yu JG, Yu XX (2008) Hydrothermal synthesis and photocatalytic activity of zinc oxide hollow spheres. *Environ Sci Technol* 42:4902–4907
- Zhang L, Wong KH, Zhang DQ, Hu C, Yu JC, Chan QY, Wong PK (2009) Zn:In(OH)₃S_z solid solution nanoplates: synthesis, characterization, and photocatalytic mechanism. *Environ Sci Technol* 43:7883–7888
- Zhao Y, Yuan M, Chen Y, Yan Xu JL, Huang YP, Lian JB, Bao J, Qiu JX, Xu L, Xu YG, Xu H, Li HM (2018) Construction of molybdenum dioxide nanosheets coated on the surface of nickel ferrite nanocrystals with ultrahigh specific capacity for hybrid supercapacitor. *Electrochim Acta* 206:439–448

Publisher's Note Springer Nature remains neutral with regard to jurisdictional claims in published maps and institutional affiliations.